Single-Mode Photon Blockade Enhanced by Bi-Tone Drive

Ming Li,[1,2,*] Yan-Lei Zhang,[1,2,*] Shu-Hao Wu,[3] Chun-Hua Dong,[1,2] Xu-Bo Zou,[1,2]
Guang-Can Guo,[1,2] and Chang-Ling Zou[1,2,†]

[1]*CAS Key Laboratory of Quantum Information, University of Science and Technology of China, Hefei 230026, China*
[2]*CAS Center For Excellence in Quantum Information and Quantum Physics, University of Science and Technology of China, Hefei, Anhui 230026, People's Republic of China*
[3]*Department of Physics, University of Oregon, Eugene, Oregon 97403, USA*

(Received 17 December 2021; revised 18 June 2022; accepted 6 July 2022; published 18 July 2022)

A scheme for observing photon blockade in a single bosonic mode with weak nonlinearity is proposed and numerically verified. Using a simple bi-tone drive, sub- and super-Poissonian light can be generated with high fidelity. With a periodically poled lithium niobate microcavity, a sub-Poissonian photon source with kHz count rate can be realized. Our proposed scheme is robust against parameter variations of the cavity and extendable to any bosonic system with anharmonic energy levels.

DOI: 10.1103/PhysRevLett.129.043601

Introduction.—Photon blockade originates from the anharmonic dynamics of bosonic modes and has been used for generating optical fields with nonclassical statistics [1–4] and building photonic quantum gates [5–7]. It relies on the strong nonlinear couplings of a bosonic mode to other bosonic modes such as photonic resonators [7–11], mechanical oscillators [12–16], polaritons [17] as well as single-photon emitters [18] such as neutral atoms [1,2,19,20], quantum dots [21,22], and superconducting qubits [23–25]. To block the excitation of multiphoton states, it is desired that the photon-number anharmonicity surpasses the linewidth of the mode or emitter, which remains difficult to obtain in systems that possess weak inherent nonlinearity.

In a weakly coupled nonlinear system, unconventional photon blockade [26–28] has been proposed to suppress the multiphoton population by utilizing the quantum interference between different paths of transitions [29,30]. Such a scheme requires an additional degree of freedom of photons, such as an ancillary photonic mode or emitter to provide an extra dimension for the construction of different transition pathways [31]. The multimode configuration has been theoretically proposed in a variety of physical systems [32–37] and experimentally realized in the quantum dot cavity quantum electrodynamics system [38] and superconducting resonators [39]. However, it not only raises difficulties for the detection of quantum optical fields but also has demanding requirements on the device parameters. Photon blockade in a single bosonic mode has been proposed by controlling the temporal property of the coherent optical fields [40–42]. In such schemes, the restriction on the photonic device is transferred to the pump laser, which to some extent increases the experimental feasibility. Nevertheless, a special pulse shape or parametric drive was needed and the multiphoton populations were not suppressed completely with only coherent input.

In this Letter, we propose a mechanism for near-perfect photon blockade in an optical cavity with weak anharmonicity. By constructing the interference of excitation paths to a Fock state via multiple drives with different frequencies, the two-photon population of a Kerr oscillator is canceled, generating a sub-Poissonian light with near-zero second-order quantum correlation. Our scheme only requires a coherent laser stably locked to the cavity resonance and an electro-optical modulator, thus is experimentally feasible for current experimental platforms and leads to atom-free or junction-free demonstration of quantum effects in integrated photonics platforms [43–45].

Model and principle.—Figure 1(a) shows the proposed scheme for observing the photon blockade effect in a weakly anharmonic bosonic cavity. The bi-tone laser is generated from a continuous-wave laser (frequency ω_p) by an electro-optical modulator, with the frequency (ω_s), amplitude, and phase of the sideband controlled by a stable radio-frequency (rf) drive. Then two laser tones are injected into a cavity filled with medium with weak nonlinearity, which could be offered by either the bulky $\chi^{(2)}$ or $\chi^{(3)}$ nonlinearities, the photon-emitter ensemble or the photon-phonon interactions. The system exhibits anharmonicity as the energy level depends on the system excitation number. The quantum statistical properties of the output field could be characterized by the coincidence detected by two single-photon detectors after a beam splitter.

Without loss of generality, we first consider the simplest and widely studied nonlinear system, i.e., a cavity filled with Kerr material. Driven by a bi-tone coherent field, the system Hamiltonian is ($\hbar = 1$) [11]

$$H = \omega_a a^\dagger a + g a^{\dagger 2} a^2 + (\varepsilon_p a^\dagger e^{-i\omega_p t} + \varepsilon_s a^\dagger e^{-i\omega_s t} + \text{H.c.}), \tag{1}$$

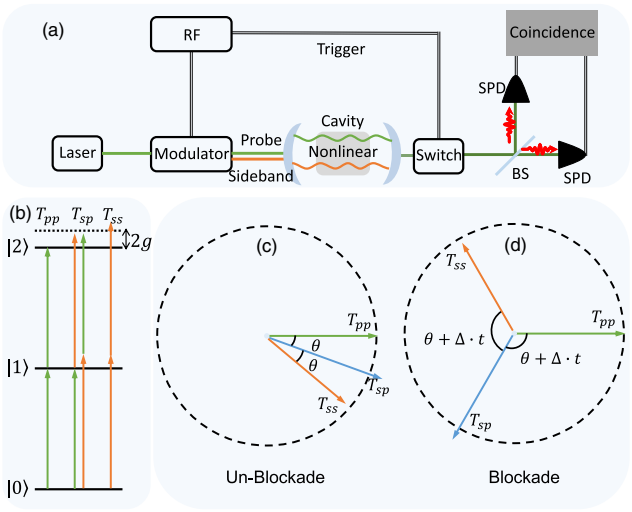

FIG. 1. (a) Setup of the proposed scheme. A coherent laser together with a sideband derived from an electro-optical modulator is injected into a cavity with weak nonlinearity. The outgoing field from the cavity is gated by an optical switch and subsequently characterized by a pair of single-photon detectors for coincidence measurement. Beam splitter (BS). Single-photon detector (SPD). (b) Energy levels of an anharmonic bosonic mode and the possible transition pathways. g is the figure of merit of the anharmonicity. (c) and (d) The polar coordinates representations of transition amplitudes of different pathways at different times.

where a ($a^\dagger$) is the annihilation (creation) operator of the bosonic mode, ω_a is the resonant frequency, g describes the anharmonicity of the system, and ε_j is the drive field with frequencies of ω_j and $j \in \{p, s\}$ for probe or sideband [Fig. 1(a)]. Because of the Kerr nonlinear interaction, the frequency of Fock state $|2\rangle$ is slightly shifted away from the bare harmonic resonance by $2g$, as shown by Fig. 1(b).

For a very weak anharmonicity $g \ll \kappa$ (κ is the mode amplitude dissipation rate), the photon blockade effect is almost undetectable under monochromatic excitation. In the presence of a bi-tone drive, the Fock state $|0\rangle$ can be excited to $|2\rangle$ via different paths, i.e., absorbing two photons from the same laser or one photon from each laser with different frequencies, as indicated by the green and orange arrows in Fig. 1(b). To the limit of weak excitation $|\varepsilon_{p,s}| \ll \kappa$, the excitation of high photon number states can be neglected and the amplitude $\alpha_2(t)$ of Fock state $|2\rangle$ can be analytically solved following the Schrödinger equation as [46]

$$\alpha_2(t) = T_{pp} + T_{sp}\frac{\varepsilon_s}{\varepsilon_p}e^{-i\Delta_s t} + T_{ss}\frac{\varepsilon_s^2}{\varepsilon_p^2}e^{-2i\Delta_s t}, \quad (2)$$

where $T_{pp,sp,ss}$ denote the transition amplitudes of the corresponding paths in Fig. 1(b). All transition amplitudes are proportional to the square of the laser amplitude ε_p^2, and also depend on the relative detuning between the drive laser and the energy level, and the cavity dissipation rate. The phases of different paths are inhomogeneous to the drive frequency and also include the contribution of the initial phase $\arg(\varepsilon_s/\varepsilon_p)$ of the bi-tone input as well as the accumulated phase $\Delta_s t$ due to the frequency detuning $\Delta_s = \omega_s - \omega_p$. Therefore, these three amplitudes may interfere destructively and lead to a vanished population of Fock state $|2\rangle$, shown by Fig. 1(d). The result is the blockaded optical field with near-zero second-order correlation function with the driving strengths fulfilling

$$\left|\frac{\varepsilon_s}{\varepsilon_p}\right| = \left|\frac{-T_{sp} \pm \sqrt{T_{sp}^2 - 4T_{pp}T_{ss}}}{2T_{pp}}\right|, \quad (3)$$

at the instant of

$$t_s = \frac{2m\pi + \arg(\varepsilon_s/\varepsilon_p) - \arg(\varepsilon)}{\Delta_s}, \quad (4)$$

with $m \in \mathbb{Z}$ and ε denoting the term inside the vertical bar on the right side of Eq. (3). For weak drive fields, the ratio in Eq. (3) is drive independent. The first term in the numerator of Eq. (4) indicates a periodic appearance of photon blockade. The second term is the external phase of the sideband laser, and the third term is due to the anharmonic response of the nonlinear cavity.

Two-photon blockade.—The dynamics of the open system are investigated by numerically solving the time-dependent master equation [47] $d\rho/dt = -i[H, \rho] + \kappa(2a\rho a^\dagger - a^\dagger a\rho - \rho a^\dagger a)$, where ρ is the density matrix of the cavity field. The photon blockade is evaluated by the equal-time second-order quantum correlation function $g^{(2)}(t) = \langle a^\dagger(t)a^\dagger(t)a(t)a(t)\rangle / \langle a^\dagger(t)a(t)\rangle^2$, as shown in Fig. 2(a). In the simulation, the weak Kerr coupling strength is set $g = 10^{-2}\ \kappa$ and the amplitude of the bi-tone field is set according to the optimal condition of $\varepsilon_s/\varepsilon_p$ by Eq. (3). For most of the time, the $g^{(2)}(t)$ is near 1, reflecting the weak anharmonicity of the mode. As indicated by the sharp oscillation of $g^{(2)}(t)$, significant quantum interference can be observed at special instants as predicted by Eq. (4). The sub-Poissonian statistics corresponds to the destructive interference between different transition amplitudes. The minimum of $g^{(2)}(t)$ is near zero, in contrast to $g^{(2)}(t) = 0.9999$ for a single-tone probe. The simulation is performed in a 10-dimension truncated Fock state space, showing good agreement with the analytical prediction. We note that the cyclical appearance of sub-Poissonian statistics seems similar to the pulse-driven dynamical photon blockade in Ref. [40]. Differently, we introduce a new degree of freedom, i.e., the photon frequency, to control the system dynamics, which requires only a minimal resource and reveals the essential physics of dynamical photon blockade. In the current unified picture, the pulse trains utilized in

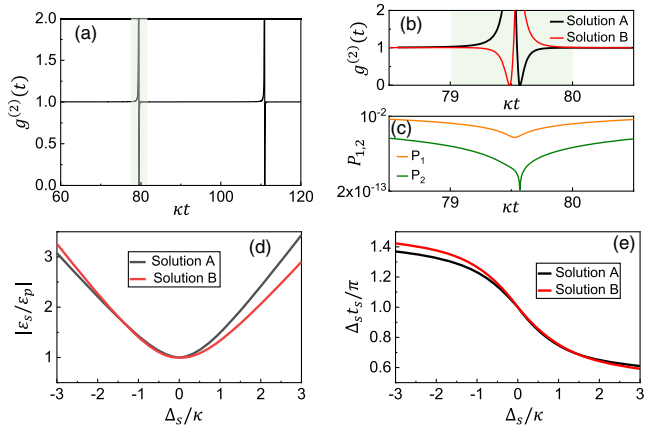

FIG. 2. (a) The dynamics of the equal-time second-order quantum correlation function $g^{(2)}(t)$. (b) Zoom-in view of $g^{(2)}(t)$ near the interference region for two solutions of Eq. (3). (c) Populations of Fock states $|1\rangle$ (P_1) and $|2\rangle$ (P_2). (d)–(e) The amplitude ratios $|\varepsilon_s/\varepsilon_p|$ of the two laser tones and the corresponding phases $\Delta_s t_s$ under optimal blockade conditions of the cavity field with $g/\kappa = 10^{-2}$. The initial phase of the bi-tone laser is set as $\arg(\varepsilon_s/\varepsilon_p) = 0$.

Ref. [40] are essentially equivalent to a drive with multiple laser tones. Because of the simplicity, our protocol gives clear analytical expression of the optimal blockade conditions, which can be easily generalized to the generation of other quantum states. As a result, our protocol achieves a much smaller $g^{(2)}(t)$ function. For unconventional and dynamical photon blockade in weakly nonlinear systems, the high-fidelity antibunching effect requires the high photon number states not to be excited significantly, which limits the ultimate photon occupation number [Fig. 2(c)].

According to Eq. (4), the periodic blockade instant can be tuned by the initial phase $\arg(\varepsilon_s/\varepsilon_p)$ of the bi-tone laser through the rf drive. Meanwhile, the sub-Poissonian light can be filtrated from the coherent laser background on demand by controlling the triggered delay from the same rf signal [Fig. 2(a)]. Even though the phase fluctuations of the laser tones might drift the interference time, the trigger controlled by the same rf signal can synchronize the working time of the optical switch in real-time without feedback according to the optimal blockade condition [Eq. (4)]. Our protocol is thus immune to the relative parameter fluctuations of the laser tones. Compared with the unconventional photon blockade [27], which demands precise tuning of the frequencies and couplings of the cavity modes, the current photon blockade scheme is more feasible for experimental implementation by simply tuning the frequency and amplitude of the rf drive.

As inferred from Eq. (3), for a given probe field with strength ε_p, there always exist two optimal conditions of the sideband ε_s for realizing perfect photon blockade. The behavior of the $g^{(2)}(t)$ around the optimal instants for the two solutions are presented in Figs. 2(b), showing a peak before and after the photon blockade, respectively. The interference-induced bunching and antibunching effects are attributed to the nonsimultaneous minimum point of the populations of Fock states $|2\rangle$ and $|1\rangle$ [Fig. 2(c)]. Figures 2(d)–2(e) show the optimal amplitude ratios $|\varepsilon_s/\varepsilon_p|$ and the corresponding phases $\arg(\varepsilon_s/\varepsilon_p)$ of the input laser for different probe detunings Δ_s. Since the amplitudes of different transition paths are proportional to the corresponding strength of the input field, $|\varepsilon_s/\varepsilon_p|$ must be increased with $|\Delta_s|$ to balance T_{pp}, T_{sp}, and T_{ss}. It can be seen from Fig. 2(d) that for small frequency difference between two laser tones, i.e., $\Delta_s \ll \kappa$, the amplitude of the sideband only slightly deviates from the pump field. While for a larger detuning Δ_s, the driving strength ε_s must be increased to be larger than ε_p. Meanwhile, the response of the cavity also differs for different Δ_s, and thus the phase $\Delta_s t_s$ does not remain an constant value, as indicated by Fig. 2(e).

It should be noted that, the sharp oscillation of $g^{(2)}(t)$ in Fig. 2 implies the quantum interference might be parameter sensitive. It is critical to investigate the width of the time window, as well as their tolerance on the parameter uncertainties for practical experiments. In essence, the photon blockade effect in our scheme originates from the inhomogeneous response of different transition paths to the photon frequency due to the anharmonicity. However, the inhomogeneity decreases with a reduced nonlinear coupling rate g. Here, we define the time window of the temporal photon blockade ΔT as the duration within which $g^{(2)}(t) \leq 0.95$. We carefully investigate its dependence on the nonlinearity g and the blockade repetition rate Δ_s. As shown in Fig. 3(a), for both optimal conditions according to Eq. (3), ΔT is proportional to the nonlinear coupling rate. Under an extremely weak nonlinearity $g/\kappa = 10^{-3}$, ΔT could be even as large as 0.05 times the cavity lifetime. The width of the time window is proportional to the photon emission rate of the nonclassical source. Notably, since the blockade instant appears periodically with the frequency Δ_s, one may expect to increase the duty cycle of time for more nonclassical fields under large frequency detuning of the sideband. Figure 3(b) shows a negative relationship between the repetition rate Δ_s and ΔT at optimal conditions. This trade-off relation might imply a correspondence between the amount of quantum resource and optical nonlinearity, which is worth further investigations in the future [48].

The robustness of the photon blockade scheme is crucial for practical experiments, and the main challenges come from the instability of the lasers and the cavity mode, as illustrated in Fig. 3(c). We note that our scheme is immune to the fluctuation of Δ_s, as it is synchronized to the switch by the rf source. However, both the detuning between the cavity mode and the input probe laser and the amplitude ratio $|\varepsilon_s/\varepsilon_p|$ of the input lasers might fluctuate and deviate from the optimal value. Therefore, Fig. 3(d) investigates the

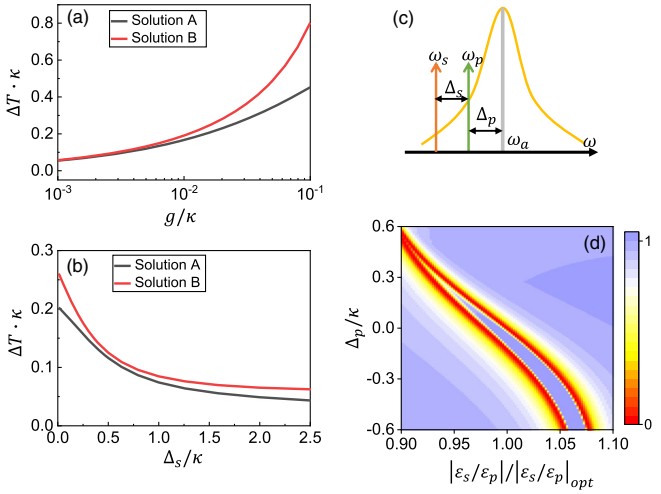

FIG. 3. The time window of the temporal photon blockade and their tolerance to experimental parameter variations. (a)–(b) Relationship between the time window ΔT for $g^{(2)}(t) \leq 0.95$ under different nonlinear coupling rate g and detuning Δ_s between the two laser tones. (c) Illustration of the frequencies of the lasers and cavity mode. (d) The minimum correlation function $g^{(2)}_{\min}$ for different pump laser detunings Δ_p and amplitude ratios $|\varepsilon_s/\varepsilon_p|$ of the bi-tone laser. $|\varepsilon_s/\varepsilon_p|_{\text{opt}}$ is the amplitude ratio under the optimal blockade condition.

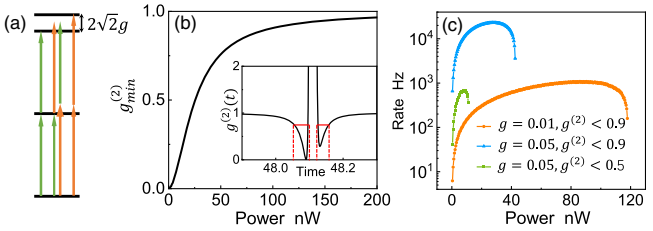

FIG. 4. Photon blockade in a $\chi^{(2)}$ microcavity. (a) Illustration of the energy levels and possible transition paths under excitation of a bi-tone laser. (b) Relationship between the input power and the minimum second-order correlation $g^{(2)}_{\min}$. The interference is shown by the oscillation in the inset. (c) The photon emission rate of the sub-Poissonian light under different pump powers. The emission field is triggered by an optical switch to select photons with $g^{(2)}(t) < 0.9$ (brown and blue lines) and $g^{(2)}(t) < 0.5$ (green line).

parameter dependence of the minimum of second-order correlation $g^{(2)}_{\min}$ on Δ_p and $|\varepsilon_s/\varepsilon_p|$. Here, we set $g/\kappa = 10^{-2}$ and change the driving strength $|\varepsilon_s/\varepsilon_p|$ around the optimal value $|\varepsilon_s/\varepsilon_p|_{\text{opt}}$ derived from Eq. (3) with $\Delta_s = 0.2\ \kappa$. As can be seen from the red stripes in the density map [Fig. 3(d)], a frequency fluctuation at the order of 1% κ and a relative laser amplitude fluctuation $|\varepsilon_p/\varepsilon_s|$ at the order of 1% are tolerable, indicating high robustness of our bi-tone scheme.

Experimental feasibility with $\chi^{(2)}$ microcavity.—The bi-tone enhanced photon blockade scheme is universal for anharmonicity induced by photon-atom interaction or photon-photon coherent interaction. Recently, single-photon anharmonicity g/κ ratio exceeding 0.01 is reported on a photonic chip, by designing periodically poled lithium niobate (PPLN) [43,44] and indium gallium phosphide (InGaP) [45] microring cavities for an optimized degenerate $\chi^{(2)}$ interaction between two optical modes. Therefore, such platforms of nonlinear microresonators hold great potential for room-temperature quantum information processing [7,49–52] and is promising for demonstrating our scheme. As shown in Fig. 4(a), the energy levels of the combined Fock states of the fundamental (a) and second-harmonic (b) modes exhibit anharmonicity due to the $\chi^{(2)}$ interaction $g(a^2b^\dagger + a^{\dagger 2}b)$, with g being the corresponding photon-photon coupling strength. The degeneracy of two-excitation states ($|0\rangle_a \otimes |1\rangle_b$ and $|2\rangle_a \otimes |0\rangle_b$) are lifted and the eigenstates have a energy difference of $2\sqrt{2}g$, while the single-excitation state $|1\rangle_a \otimes |0\rangle_b$ is unperturbated by the $\chi^{(2)}$ interaction. Similar to the analysis with Kerr nonlinearity, there are also different transition pathways to the two-excitation state [Fig. 4(a)], which can be engineered for destructive quantum interference [46].

Here, we perform a full numerical simulation on the optical fields based on the quantum cluster expansion method [53] using practical experimental parameters according to Ref. [43]. As shown in the inset of Fig. 4(b), a near-zero $g^{(2)}(t)$ can be obtained under perfect interference conditions predicted by analytical analysis [46]. Because two energy levels contribute to the interference, two blockade windows are found in the $\chi^{(2)}$ interaction. However, the single-photon emission rate is also limited by the destructive interference during the narrow blockade window [Fig. 4(c)]. The photon emission rate can be increased with stronger pump power at the expense of increased second-order quantum correlation $g^{(2)}_{\min}$, which tends to be 1 and recovers the quantum statistics of a coherent laser [Fig. 4(b)] due to the excitation of higher Fock states. Figure 4(c) shows the emission rate of photons during the selected time window marked by the right red-dashed frame in Fig. 4(b) with $g^{(2)}(t) < 0.9$. A single-photon counting rate over 1 kHz is achievable under a pump power of 90 nW for the experimentally demonstrated anharmonicity $g/\kappa = 0.01$ [43]. With an optimized $g/\kappa = 0.05$ in a PPLN microring with the same geometry, the emission rate can be improved by more than 1 order of magnitude (2.3×10^4 Hz) with a lower power of 20 nW [Fig. 4(c)], corresponding to an increase of photon emission probability from 9×10^{-5} to 2.3×10^{-3} per blockade window. Towards the strong coupling regime, $g/\kappa \sim 1$ is potential in phase-matched photonic crystal cavity [54] made by GaAs [55], benefit from a stronger nonlinear susceptibility and much smaller mode volume as well as a potentially high Q factor [56], our scheme would achieve a

generation rate of 0.1 MHz for $g^{(2)}(t) < 0.1$, while $g^{(2)}_{\min}$ is always larger than 0.5 for the conventional single-tone scheme.

The weak nonlinearity requires high-speed modulators to construct the time window that matches the duration of the interference. For the anharmonicity $g/\kappa \sim 0.01$ in the PPLN [43] and InGaP [45] microcavities, the time window for observing significant blockade effect can be 0.1 times the cavity lifetime, corresponding to 1 and 0.1 ns for the PPLN and InGaP microcavities with quality factors 10^7 and 10^6, respectively. The tolerable frequency fluctuation of Δ_p and time window ΔT are on the orders of 100 kHz and 10 ns, respectively. All these parameters are within the capability of commercial 10 GHz electro-optical modulators based on the current optical frequency locking and switching techniques.

Discussion and conclusion.—In conclusion, we demonstrate a universal mechanism to enhance the photon blockade of bosonic modes with weak anharmonic energy levels. Compared with previous schemes, our scheme avoids the stringent device design for the demanding requirements on frequency matching and critical coupling strengths for multiple cavities. The photon blockade is robust as it only requires a coherent laser locked to the cavity resonance and a modulated sideband generated by a rf drive. In addition to the suppression of the two-photon population in one mode, the mechanism of photon blockade is universal, and it applies to other nonlinearities among multiple modes [57] as well as the multiphoton blockades [58–60]. The blockade of other Fock states can be achieved similarly by designing the destructive interference [46]. The bi-tone drive is also extensible to a multitone drive for more powerful control of the photon statistics. We further demonstrate its experimental feasibility based on the recently reported parameters in a photonic microcavity with $\chi^{(2)}$ nonlinearity [43–45].

This work was funded by the National Key R&D Program (Grant No. 2021YFA1402004), the National Natural Science Foundation of China (Grants No. 11874342, No. 11922411, No. 12061131011, and No. 11904316), Natural Science Foundation of Anhui Province (Grants No. 2008085QA34 and No. 2108085MA17). M. L., C. L. Z., and Y. L. Z. were also supported by the Fundamental Research Funds for the Central Universities, and the State Key Laboratory of Advanced Optical Communication Systems and Networks. The numerical calculations in this Letter were partially done on the supercomputing system in the Supercomputing Center of the University of Science and Technology of China.

*These authors contributed equally to this work.
†clzou321@ustc.edu.cn

[1] K. M. Birnbaum, A. Boca, R. Miller, A. D. Boozer, T. E. Northup, and H. J. Kimble, Photon blockade in an optical cavity with one trapped atom, Nature (London) **436**, 87 (2005).
[2] B. Dayan, A. S. Parkins, T. Aoki, E. P. Ostby, K. J. Vahala, and H. J. Kimble, A photon turnstile dynamically regulated by one atom, Science **319**, 1062 (2008).
[3] J. Tang, L. Tang, H. Wu, Y. Wu, H. Sun, H. Zhang, T. Li, Y. Lu, M. Xiao, and K. Xia, Towards On-Demand Heralded Single-Photon Sources via Photon Blockade, Phys. Rev. Applied **15**, 064020 (2021).
[4] R. Huang, A. Miranowicz, J.-Q. Liao, F. Nori, and H. Jing, Nonreciprocal Photon Blockade, Phys. Rev. Lett. **121**, 153601 (2018).
[5] B. Hacker, S. Welte, G. Rempe, and S. Ritter, A photon-photon quantum gate based on a single atom in an optical resonator, Nature (London) **536**, 193 (2016).
[6] D. Tiarks, S. Schmidt-Eberle, T. Stolz, G. Rempe, and S. Dürr, A photon-photon quantum gate based on Rydberg interactions, Nat. Phys. **15**, 124 (2019).
[7] M. Li, Y.-L. Zhang, H. X. Tang, C.-H. Dong, G.-C. Guo, and C.-L. Zou, Photon-Photon Quantum Phase Gate in a Photonic Molecule with $\chi^{(2)}$ Nonlinearity, Phys. Rev. Applied **13**, 044013 (2020).
[8] A. Majumdar and D. Gerace, Single-photon blockade in doubly resonant nanocavities with second-order nonlinearity, Phys. Rev. B **87**, 235319 (2013).
[9] S. Ferretti and D. Gerace, Single-photon nonlinear optics with Kerr-type nanostructured materials, Phys. Rev. B **85**, 033303 (2012).
[10] Y. H. Zhou, X. Y. Zhang, Q. C. Wu, B. L. Ye, Z.-Q. Zhang, D. D. Zou, H. Z. Shen, and C.-P. Yang, Conventional photon blockade with a three-wave mixing, Phys. Rev. A **102**, 033713 (2020).
[11] D. Roberts and A. A. Clerk, Driven-Dissipative Quantum Kerr Resonators: New Exact Solutions, Photon Blockade and Quantum Bistability, Phys. Rev. X **10**, 021022 (2020).
[12] P. Rabl, Photon Blockade Effect in Optomechanical Systems, Phys. Rev. Lett. **107**, 063601 (2011).
[13] J.-Q. Liao and F. Nori, Photon blockade in quadratically coupled optomechanical systems, Phys. Rev. A **88**, 023853 (2013).
[14] A. Miranowicz, J. Bajer, N. Lambert, Y.-x. Liu, and F. Nori, Tunable multiphonon blockade in coupled nanomechanical resonators, Phys. Rev. A **93**, 013808 (2016).
[15] X.-W. Xu, A.-X. Chen, and Y.-x. Liu, Phonon blockade in a nanomechanical resonator resonantly coupled to a qubit, Phys. Rev. A **94**, 063853 (2016).
[16] B. Li, R. Huang, X. Xu, A. Miranowicz, and H. Jing, Nonreciprocal unconventional photon blockade in a spinning optomechanical system, Photonics Res. **7**, 630 (2019).
[17] O. Kyriienko, D. N. Krizhanovskii, and I. A. Shelykh, Nonlinear Quantum Optics with Trion Polaritons in 2d Monolayers: Conventional and Unconventional Photon Blockade, Phys. Rev. Lett. **125**, 197402 (2020).
[18] R. Trivedi, M. Radulaski, K. A. Fischer, S. Fan, and J. Vučković, Photon Blockade in Weakly Driven Cavity Quantum Electrodynamics Systems with Many Emitters, Phys. Rev. Lett. **122**, 243602 (2019).

[19] C. Hamsen, K. N. Tolazzi, T. Wilk, and G. Rempe, Two-Photon Blockade in an Atom-Driven Cavity QED System, Phys. Rev. Lett. **118**, 133604 (2017).

[20] A. Cidrim, T. S. do Espirito Santo, J. Schachenmayer, R. Kaiser, and R. Bachelard, Photon Blockade with Ground-State Neutral Atoms, Phys. Rev. Lett. **125**, 073601 (2020).

[21] A. Faraon, I. Fushman, D. Englund, N. Stoltz, P. Petroff, and J. Vučković, Coherent generation of non-classical light on a chip via photon-induced tunnelling and blockade, Nat. Phys. **4**, 859 (2008).

[22] K. Müller, A. Rundquist, K. A. Fischer, T. Sarmiento, K. G. Lagoudakis, Y. A. Kelaita, C. Sánchez Muñoz, E. del Valle, F. P. Laussy, and J. Vučković, Coherent Generation of Nonclassical Light on Chip via Detuned Photon Blockade, Phys. Rev. Lett. **114**, 233601 (2015).

[23] A. J. Hoffman, S. J. Srinivasan, S. Schmidt, L. Spietz, J. Aumentado, H. E. Türeci, and A. A. Houck, Dispersive Photon Blockade in a Superconducting Circuit, Phys. Rev. Lett. **107**, 053602 (2011).

[24] C. Lang, D. Bozyigit, C. Eichler, L. Steffen, J. M. Fink, A. A. Abdumalikov, M. Baur, S. Filipp, M. P. da Silva, A. Blais, and A. Wallraff, Observation of Resonant Photon Blockade at Microwave Frequencies Using Correlation Function Measurements, Phys. Rev. Lett. **106**, 243601 (2011).

[25] J. Tang, Y. Wu, Z. Wang, H. Sun, L. Tang, H. Zhang, T. Li, Y. Lu, M. Xiao, and K. Xia, Vacuum-induced surface-acoustic-wave phonon blockade, Phys. Rev. A **101**, 053802 (2020).

[26] T. C. H. Liew and V. Savona, Single Photons from Coupled Quantum Modes, Phys. Rev. Lett. **104**, 183601 (2010).

[27] H. Flayac and V. Savona, Unconventional photon blockade, Phys. Rev. A **96**, 053810 (2017).

[28] E. Zubizarreta Casalengua, J. C. López Carreño, F. P. Laussy, and E. d. Valle, Conventional and unconventional photon statistics, Laser Photonics Rev. **14**, 1900279 (2020).

[29] M. Bamba, A. Imamoğlu, I. Carusotto, and C. Ciuti, Origin of strong photon antibunching in weakly nonlinear photonic molecules, Phys. Rev. A **83**, 021802(R) (2011).

[30] C.-L. Zou, L. Jiang, X.-B. Zou, and G.-C. Guo, Filtration and extraction of quantum states from classical inputs, Phys. Rev. A **94**, 013841 (2016).

[31] K. Hou, C. J. Zhu, Y. P. Yang, and G. S. Agarwal, Interfering pathways for photon blockade in cavity QED with one and two qubits, Phys. Rev. A **100**, 063817 (2019).

[32] D. Gerace and V. Savona, Unconventional photon blockade in doubly resonant microcavities with second-order nonlinearity, Phys. Rev. A **89**, 031803(R) (2014).

[33] Y. H. Zhou, H. Z. Shen, and X. X. Yi, Unconventional photon blockade with second-order nonlinearity, Phys. Rev. A **92**, 023838 (2015).

[34] H. Flayac, D. Gerace, and V. Savona, An all-silicon single-photon source by unconventional photon blockade, Sci. Rep. **5**, 11223 (2015).

[35] O. Kyriienko and T. C. H. Liew, Triggered single-photon emitters based on stimulated parametric scattering in weakly nonlinear systems, Phys. Rev. A **90**, 063805 (2014).

[36] D. Stefanatos and E. Paspalakis, Efficient entanglement generation between exciton-polaritons using shortcuts to adiabaticity, Opt. Lett. **43**, 3313 (2018).

[37] H. Lin, H. Yang, X. Wang, Y. Zhou, and Z. Yao, Realization of the unconventional photon blockade based on a three-wave mixing system, Opt. Express **29**, 8235 (2021).

[38] H. J. Snijders, J. A. Frey, J. Norman, H. Flayac, V. Savona, A. C. Gossard, J. E. Bowers, M. P. van Exter, D. Bouwmeester, and W. Löffler, Observation of the Unconventional Photon Blockade, Phys. Rev. Lett. **121**, 043601 (2018).

[39] C. Vaneph, A. Morvan, G. Aiello, M. Féchant, M. Aprili, J. Gabelli, and J. Estève, Observation of the Unconventional Photon Blockade in the Microwave Domain, Phys. Rev. Lett. **121**, 043602 (2018).

[40] S. Ghosh and T. C. H. Liew, Dynamical Blockade in a Single-Mode Bosonic System, Phys. Rev. Lett. **123**, 013602 (2019).

[41] G. H. Hovsepyan, A. R. Shahinyan, and G. Y. Kryuchkyan, Multiphoton blockades in pulsed regimes beyond stationary limits, Phys. Rev. A **90**, 013839 (2014).

[42] L. Andrew, R. David, and A. A. Clerk, Unconditional Fock state generation using arbitrarily weak photonic nonlinearities, Sci. Adv. **7**, eabj1916 (2021).

[43] J. Lu, M. Li, C.-L. Zou, A. A. Sayem, and H. X. Tang, Toward 1% single-photon anharmonicity with periodically poled lithium niobate microring resonators, Optica **7**, 1654 (2020).

[44] J.-Y. Chen, Z. Li, Z. Ma, C. Tang, H. Fan, Y. M. Sua, and Y.-P. Huang, Photon Conversion and Interaction in a Quasi-Phase-Matched Microresonator, Phys. Rev. Applied **16**, 064004 (2021).

[45] M. Zhao and K. Fang, InGaP quantum nanophotonic integrated circuits with 1.5% nonlinearity-to-loss ratio, Optica **9**, 258 (2022).

[46] See Supplemental Material at http://link.aps.org/supplemental/10.1103/PhysRevLett.129.043601 for theoretical derivations.

[47] D. F. Walls and G. J. Milburn, *Quantum Optics* (Springer Science & Business Media, Berlin, Heidelberg, 2007).

[48] S. Deffner and S. Campbell, Quantum speed limits: From Heisenberg's uncertainty principle to optimal quantum control, J. Phys. A **50**, 453001 (2017).

[49] S. Krastanov, M. Heuck, J. H. Shapiro, P. Narang, D. R. Englund, and K. Jacobs, Room-temperature photonic logical qubits via second-order nonlinearities, Nat. Commun. **12**, 191 (2021).

[50] F. Shi, X. Rong, N. Xu, Y. Wang, J. Wu, B. Chong, X. Peng, J. Kniepert, R.-S. Schoenfeld, W. Harneit *et al.*, Room-Temperature Implementation of the Deutsch-Jozsa Algorithm with a Single Electronic Spin in Diamond, Phys. Rev. Lett. **105**, 040504 (2010).

[51] V. Venkataraman, K. Saha, and A. L. Gaeta, Phase modulation at the few-photon level for weak-nonlinearity-based quantum computing, Nat. Photonics **7**, 138 (2013).

[52] B. Náfrádi, M. Choucair, K.-P. Dinse, and L. Forró, Room temperature manipulation of long lifetime spins in metallic-like carbon nanospheres, Nat. Commun. **7**, 1 (2016).

[53] Y.-X. Huang, M. Li, K. Lin, Y.-L. Zhang, G.-C. Guo, and C.-L. Zou, Classical-to-quantum transition in multimode nonlinear systems with strong photon-photon coupling, Phys. Rev. A **105**, 043707 (2022).

[54] M. Minkov, D. Gerace, and S. Fan, Doubly resonant χ (2) nonlinear photonic crystal cavity based on a bound state in the continuum, Optica **6**, 1039 (2019).

[55] S. Buckley, M. Radulaski, K. Biermann, and J. Vučković, Second harmonic generation in photonic crystal cavities in (111)-oriented GaAs, Appl. Phys. Lett. **103**, 211117 (2013).

[56] L. Chang, A. Boes, P. Pintus, J. D. Peters, M. Kennedy, X.-W. Guo, N. Volet, S.-P. Yu, S. B. Papp, and J. E. Bowers, Strong frequency conversion in heterogeneously integrated GaAs resonators, APL Photonics **4**, 036103 (2019).

[57] S. Chakram, K. He, A. V. Dixit, A. E. Oriani, R. K. Naik, N. Leung, H. Kwon, W.-L. Ma, L. Jiang, and D. I. Schuster, Multimode photon blockade, Nat. Phys. (2022)..

[58] C. J. Villas-Boas and D. Z. Rossatto, Multiphoton Jaynes-Cummings Model: Arbitrary Rotations in Fock Space and Quantum Filters, Phys. Rev. Lett. **122**, 123604 (2019).

[59] A. Miranowicz, M. Paprzycka, Y.-x. Liu, J. Bajer, and F. Nori, Two-photon and three-photon blockades in driven nonlinear systems, Phys. Rev. A **87**, 023809 (2013).

[60] F. Zou, X.-Y. Zhang, X.-W. Xu, J.-F. Huang, and J.-Q. Liao, Multiphoton blockade in the two-photon Jaynes-Cummings model, Phys. Rev. A **102**, 053710 (2020).